

Red-emitting InP quantum dot micro-disk lasers epitaxially grown on (001) silicon

WEI LUO,^{1,†} LIYING LIN,^{1,†} JIE HUANG,¹ YU HAN,¹ AND KEI MAY LAU^{1,*}

¹Department of Electronic and Computer Engineering, Hong Kong University of Science and Technology, Clear Water Bay, Kowloon, Hong Kong, China

*Corresponding author: eekmlau@ust.hk

Received 13 July 2021; revised 13 August 2021; accepted 13 August 2021; posted 18 August 2021 (Doc. ID 436320); published 7 September 2021

Direct epitaxy of InP quantum dot (QD) lasers on silicon (Si) provides an on-chip red laser source for integrated Si photonics with different applications. Here, we demonstrate the first, to the best of our knowledge, InP QD lasers directly grown on (001) Si. Combining highly emissive InP QDs and a GaAs/Si template with low defect density, continuous-wave (CW) lasing of micro-disk lasers (MDLs) on Si is achieved at room temperature. The lowest threshold of MDLs on Si is ~ 500 nW, without considering the micro-disk surface absorption efficiency of the pump power. The MDLs grown on the native GaAs substrate with the same growth and fabrication process are compared using statistical data analysis. Similar material characterization results and device performances on these two substrates further confirm the performance of QD lasers on Si. This demonstration paves the way for future realization of integrated photonic circuits with red and near-infrared (NIR) lasers on Si. © 2021 Optical Society of America

<https://doi.org/10.1364/OL.436320>

Silicon (Si) photonics has emerged as a distinctive platform with many optical components integrated for applications of optical communication [1,2], bio-photonics [3,4], sensing [5,6], etc. Leveraging the well-established complementary metal-oxide-semiconductor (CMOS) techniques, low-cost and compact optical devices, including photodetectors [7,8] and modulators [9], have been demonstrated on Si and included in commercial Si photonics foundry services. Lasers grown on native substrates and then bonded on Si have also been commercialized. Direct epitaxy of lasers on Si offers the ultimate solution that is more compatible with the foundry process. Although the lattice mismatch between III–V materials and Si induces crystal defects [10], many epitaxial growth techniques have been developed to reduce them effectively [11,12]. To further mitigate the influence of defects on Si, quantum dots (QDs), presumably less vulnerable to defects due to discrete distribution and strong carrier confinement [13,14], are introduced as the active material. Compared with quantum well (QW) lasers, QD lasers grown on Si have shown superior performance in threshold current [15], temperature stability [16–18], gain bandwidth [19,20], etc.

Different from InAs QDs used in datacom and telecom lasers emitting at 1.3 μm and 1.55 μm [21,22], the emitting

wavelength of InP QDs covers the red and near-infrared (NIR) range [23,24] with potential applications, such as display [25], underwater communication [26], and molecular diagnostics [27]. InP QD lasers grown on native GaAs substrates have been previously demonstrated with impressive performances [24,28]. Huang *et al.* have reported InP QD lasers emitting at 660 nm on (001) GaAs substrate with 6° -toward the (111)A direction [29]. InP QD mode-locked lasers emitting at 730 nm have also been demonstrated on (001) GaAs substrate with 10° -toward the (111)A direction [30]. Recently, Dhingra *et al.* reported the growth of InP QDs on Si by molecular beam epitaxy (MBE) with a QD density of $1.3 \times 10^{11}/\text{cm}^2$ [31]. However, there has been no report of InP QD lasers grown on Si yet.

In this Letter, we demonstrate InP QD lasers grown directly on a commercial nominal (001) Si substrate. Micro-disk lasers (MDLs), having the advantages of a high-quality factor (Q-factor) and a small footprint [32], are fabricated and pumped by a 514 nm continuous-wave (CW) laser at room temperature. The power-dependent micro-photoluminescence (μPL) of the MDLs was measured to characterize the device performance. Ultra-low thresholds of ~ 500 nW were achieved on the MDLs with a diameter of 1.5 μm grown on a GaAs/Si template. For a fair comparison, statistical analysis of the MDLs grown on both GaAs substrates and the GaAs/Si templates was performed.

The InP QD laser structure was grown on a GaAs/Si templates in a horizontal reactor metal-organic chemical vapor deposition (MOCVD) system (AIXTRON 200/4). The GaAs/Si templates were grown in another MOCVD system (AIXTRON CCS) starting with a 1 μm GaAs thin-film grown on (001) Si with three-step growth (growth temperatures of 380°C, 510°C, and 560°C, respectively). Then, four cycles of thermal cycle annealing (TCA) were performed with temperatures ramping up and down between 330°C and 685°C. To further decrease the defect density, three sets of ten periods 9.5 nm $\text{In}_{0.16}\text{Ga}_{0.84}\text{As}/12$ nm GaAs strained-layer superlattices (SLSs) were inserted with a 300 nm GaAs spacer between each set. The total thickness of the GaAs/Si template was 2.75 μm with a surface roughness of ~ 3.9 nm measured by an atomic force microscope (AFM). A plan-view transmission electron microscope (TEM) characterization of the GaAs/Si template shows a threading dislocation density (TDD) of $\sim 1.9 \times 10^7/\text{cm}^2$. On top of the GaAs/Si template, a 780 nm

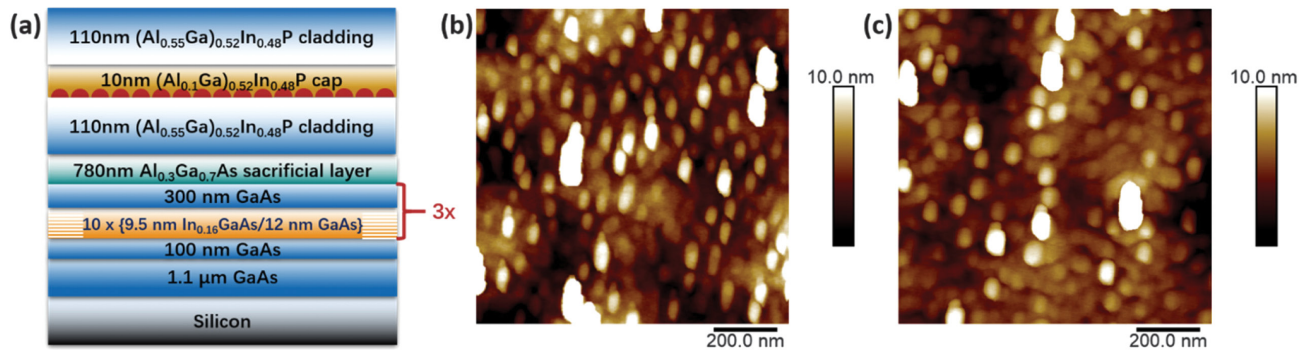


Fig. 1. (a) Schematic of the InP QD laser grown on the GaAs/Si template. AFM images of InP QDs grown on (b) the GaAs substrate and (c) the GaAs/Si template, respectively.

$\text{Al}_{0.3}\text{Ga}_{0.7}\text{As}$ sacrificial layer was grown at 710°C , followed by a 110 nm $(\text{Al}_{0.55}\text{Ga})_{0.52}\text{In}_{0.48}\text{P}$ cladding grown at the same temperature. Then 3.2 ML InP QDs were grown at 690°C and capped by 10 nm $(\text{Al}_{0.1}\text{Ga})_{0.52}\text{In}_{0.48}\text{P}$ at the same temperature. Finally, a 110 nm $(\text{Al}_{0.55}\text{Ga})_{0.52}\text{In}_{0.48}\text{P}$ cladding was grown on top of the $(\text{Al}_{0.1}\text{Ga})_{0.52}\text{In}_{0.48}\text{P}$ cap layer at 710°C . A schematic of the whole structure including the GaAs/Si template is shown in Fig. 1(a).

To characterize the morphology of the InP QDs, a layer of QDs was grown on top of the structure. The AFM images of the InP QDs grown on the GaAs substrate and the GaAs/Si template are shown in Figs. 1(b) and 1(c), respectively. The QD densities, as counted from the AFM images, on the GaAs substrate and the GaAs/Si template are $(1.3 \pm 0.05) \times 10^{10}/\text{cm}^2$ and $(1.2 \pm 0.1) \times 10^{10}/\text{cm}^2$, respectively. Some larger QDs in low density were observed on both substrates. Researchers from Stuttgart and Brunswick reported this phenomenon and studied the influence of growth parameters and GaAs offcut angles on the distributions of the two types of QDs [33,34]. The cross-sectional TEM images of the InP QD structure grown on the GaAs/Si template are shown in Figs. 2(a)–2(c). From the TEM images, the height and lateral size of the small-sized InP QDs are 4 nm and 40 nm, respectively, which are consistent with the data from the AFM measurement.

To evaluate the quality of the QDs that were grown on the GaAs substrate and the GaAs/Si template, room temperature μPL spectra of the as-grown samples without the $\text{Al}_{0.3}\text{Ga}_{0.7}\text{As}$ sacrificial layer were measured to avoid emission from the $\text{Al}_{0.3}\text{Ga}_{0.7}\text{As}$. They were pumped at $2.5 \mu\text{W}$ by a 514 nm CW diode laser with a spot diameter of $\sim 2 \mu\text{m}$.

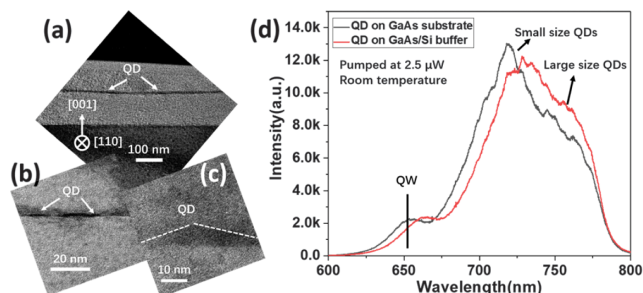


Fig. 2. (a) TEM image of the InP QDs grown on the GaAs/Si template. (b) and (c) Zoom-in TEM images of the InP QDs grown on the GaAs/Si template. (d) Room temperature μPL of the InP QDs grown on the GaAs substrate and the GaAs/Si template pumped at $2.5 \mu\text{W}$.

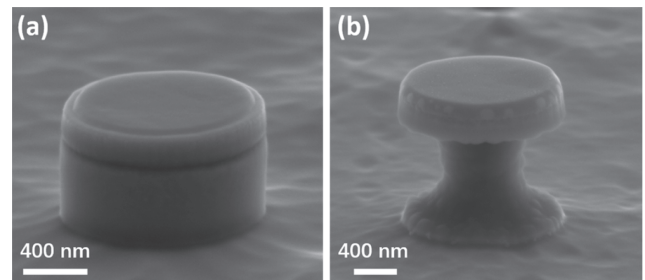


Fig. 3. 70° tilted SEM image of micro-disk lasers on the GaAs/Si template (a) before and (b) after pedestal formation.

The photoluminescence (PL) spectra in Fig. 2(d) show a dominant emission from the small-sized QDs and a shoulder at longer wavelength from the large-sized QDs [34]. The weaker PL peak near 655 nm comes from the emission of the $(\text{Al}_{0.1}\text{Ga})_{0.52}\text{In}_{0.48}\text{P}/(\text{Al}_{0.55}\text{Ga})_{0.52}\text{In}_{0.48}\text{P}$ QW. Compared with the PL of the QDs on the GaAs substrate, the PL on the GaAs/Si template is red-shifted due to the residual tensile strain caused by the introduction of SLSs and the thermal mismatch between the III–V material and Si [31]. Additionally, the PL intensities of the QDs on the two substrates are comparable.

The as-grown samples were fabricated into micro-disks with a diameter of $1.5 \mu\text{m}$. Using dispersed silica beads as the hard mask, a cylindrical pillar was formed by an inductively coupled plasma (ICP) etching process. Subsequently, the pedestal was formed by a $\text{H}_3\text{PO}_4 : \text{H}_2\text{O}_2 : \text{H}_2\text{O}$ (3 : 1 : 30) solution, which can selectively etch the $\text{Al}_{0.3}\text{Ga}_{0.7}\text{As}$ sacrificial layer. Figures 3(a) and 3(b) show the 70° tilted scanning electron microscope (SEM) images of the micro-disk on the GaAs/Si template before and after the pedestal formation. A smooth sidewall of the micro-disks was achieved, which is critical for a high-quality whisper-gallery-modes cavity.

The fabricated micro-disks were measured at room temperature with the same μPL system used for the μPL test of as-grown samples. Figures 4(a) and 4(b) show the representative power-dependent spectra of the MDLs grown on the GaAs substrate and the GaAs/Si template, respectively. At an extremely low pump power of 6.25 nW ($6.25 \times 10^{-3} P_{\text{th}}$), the mode peak has already been distinct, which reflects the QD quality and the well-defined cavity. The relatively low extinction ratio is caused by the broad emission of QDs, as shown in Fig. 2(d). The QDs emitting at different wavelengths do not contribute to the lasing and result in strong spontaneous emission [35].

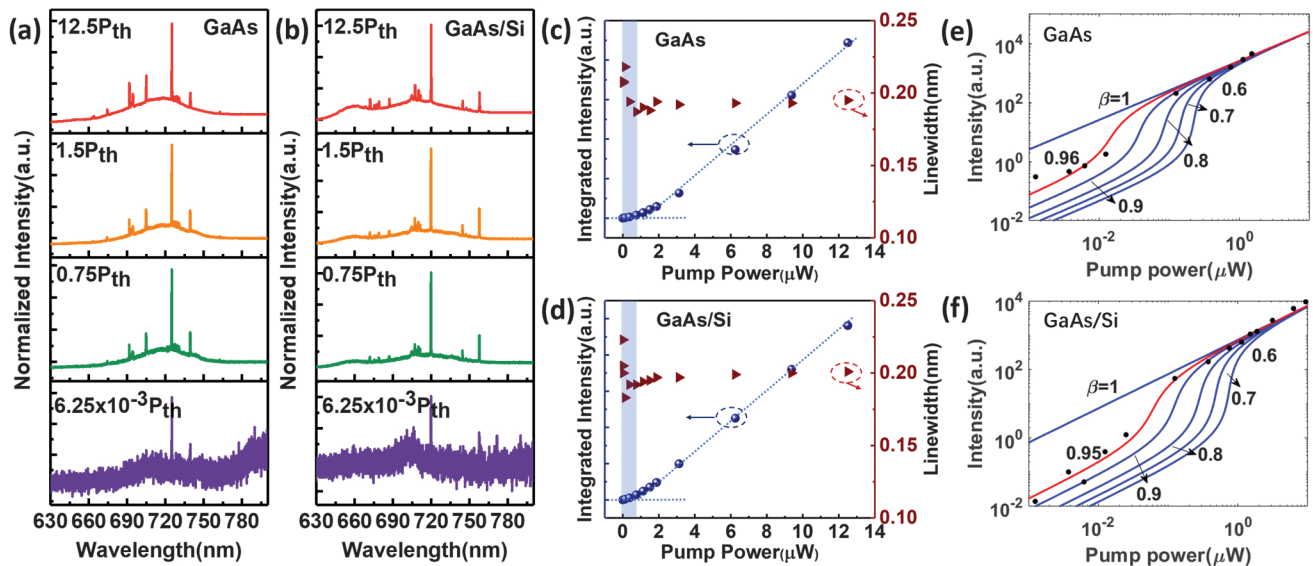


Fig. 4. Representative room temperature power-dependent PL spectra of InP QD MDLs grown on (a) the GaAs substrate and (b) the GaAs/Si template, respectively. (c) and (d) Corresponding collected PL intensity and mode linewidth of the dominant peak in (a) and (b) as a function of pump power. (e) and (f) Log–log plots of the L-L curves in (c) and (d) with β fitting.

An almost perfect overlap of the dominant mode peak and the center of spontaneous emission may also be responsible for the distinct mode peak at low pump power. In Figs. 4(c) and 4(d), the integrated PL intensity and the mode linewidth of the dominant peak are linearly plotted with increasing pump power (L-L curve). The thresholds of the two devices are extrapolated to be $\sim 1 \mu\text{W}$ without considering the micro-disk surface absorption efficiency of the pump power [36]. The linewidth of the lasing mode shows a clear drop near the threshold on both substrates, which also indicates the onset of stimulated emission [24]. To confirm the lasing behavior of the MDLs, L-L curves are plotted in log–log scale in Figs. 4(e) and 4(f), where the β fitting of the L-L curves was done using the method introduced in [36]. The high value of the β factors, which describe the fraction of spontaneous emission coupled into the lasing mode, is responsible for the low thresholds of MDLs. High cold cavity quality factors can then be extracted to be 3876 and 3993 for MDLs on the GaAs substrate and the GaAs/Si template accordingly. Compared with the threshold of the InP QD MDLs bonded on Si reported by Chu *et al.*, which is $30 \mu\text{W}$ after considering 42% absorption efficiency [36], the thresholds of our MDLs are much lower. This can be attributed to the high-quality QDs and indicates a high spontaneous emission rate as well [36]. Furthermore, the stability of QDs can also be confirmed by the linearly increased integrated intensity of the lasing peak under high pump power. For MDLs on both substrates, no obvious output intensity saturation is observed under pump power as high as $12.5 P_{\text{th}}$.

For a fair comparison, statistical analysis of the MDLs grown on the GaAs substrate and the GaAs/Si template is shown in Figs. 5(a) and 5(b). The numbers on top of the columns are average thresholds of the MDLs within the same dominant lasing wavelength range. The PL spectra of the as-grown samples are plotted in the background of each figure. Most of the MDLs grown on the GaAs/Si template show a longer dominant lasing wavelength than those on the GaAs substrate, which correlates well with the PL spectra of the as-grown samples. Generally,

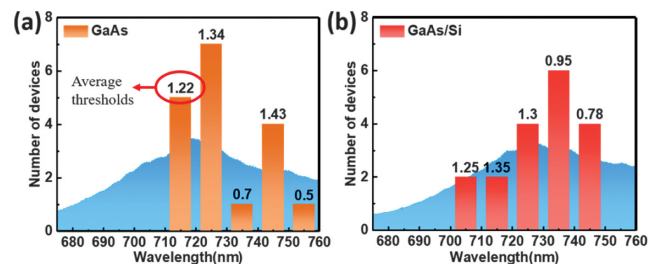


Fig. 5. Statistical analysis of the lasing behavior of InP QD MDLs grown on (a) the GaAs substrate and (b) the GaAs/Si template. The numbers on top of each column denote the average thresholds of the MDLs. The normalized PL spectra of the unprocessed samples are plotted in the background.

the thresholds of MDLs on the two substrates are comparable and all within the range of 0.5–1.5 μW , which reflects the high crystalline quality of the GaAs/Si template. Direct epitaxy of InP QDs on a high Al composition ($\text{Al}_{0.55}\text{Ga}_{0.52}\text{In}_{0.48}\text{P}$) barrier leads to higher QD density [37], which also contributes to the low threshold of the MDLs.

In conclusion, we have demonstrated the first InP QD laser grown directly on (001) Si with an ultra-low threshold of $\sim 500 \text{ nW}$ under CW optical pumping at room temperature. The MDLs on the GaAs/Si template show comparable performance as those on the native GaAs substrate, which suggests the high material quality of our GaAs/Si template and InP QDs. Future work will be concentrated on further improving the uniformity and density of the InP QDs, as well as demonstrating electrically pumped lasers on GaAs/Si templates. This monolithic solution provides an option for the integration of Si photonics with red and NIR lasers.

Funding. Innovation and Technology Fund (ITS/201/19FP).

Acknowledgment. The authors would like to thank Prof. Michael Jetter for the helpful discussions at the beginning of our InP QD research, and the

Nanosystem Fabrication Facility (NFF) and the Material Characterization & Preparation Facility (MCPF) of HKUST for their technical support.

Disclosures. The authors declare no conflicts of interest.

Data Availability. Data underlying the results presented in this Letter are not publicly available at this time but may be obtained from the authors upon reasonable request.

[†]These authors contributed equally to this Letter.

REFERENCES

- L. Vivien, et al., in *Semiconductors and Semimetals*, S. Lourdudoss, J. E. Bowers, and C. Jagadish, eds. (Elsevier, 2019), Vol. **101**, pp. 1–41.
- X. Chen, M. M. Milosevic, S. Stanković, S. Reynolds, T. D. Bucio, K. Li, D. J. Thomson, F. Gardes, and G. T. Reed, *Proc. IEEE* **106**, 2101 (2018).
- J. G. Wangüemert-Pérez, A. Hadij-Elhouati, A. Sánchez-Postigo, J. Leuermann, D.-X. Xu, P. Cheben, A. Ortega-Moñux, R. Halir, and Í. Molina-Fernández, *Opt. Laser Technol.* **109**, 437 (2019).
- P. Steglich, M. Hülsemann, B. Dietzel, and A. Mai, *Molecules* **24**(3), 519 (2019).
- C. V. Poulton, A. Yaacobi, D. B. Cole, M. J. Byrd, M. Raval, D. Vermeulen, and M. R. Watts, *Opt. Lett.* **42**(20), 4091 (2017).
- C. Ranacher, C. Consani, N. Vollert, A. Tortschanoff, M. Bergmeister, T. Grille, and B. Jakoby, *IEEE Photon. J.* **10**, 1 (2018).
- Y. Baumgartner, D. Caimi, M. Sousa, M. Hopstaken, Y. Salamin, B. Baeuerle, B. I. Bitachon, J. Leuthold, J. Faist, B. J. Offrein, and L. Czornomaz, *Opt. Express* **29**(1), 509 (2021).
- S. Mauthe, Y. Baumgartner, M. Sousa, Q. Ding, M. D. Rossell, A. Schenk, L. Czornomaz, and K. E. Moselund, *Nat. Commun.* **11**, 4565 (2020).
- R. Amin, R. Maiti, Y. Gui, C. Suer, M. Miscuglio, E. Heidari, R. T. Chen, H. Dalir, and V. J. Sorger, *Optica* **7**(4), 333 (2020).
- Q. Li and K. M. Lau, *Prog. Cryst. Growth Charact. Mater.* **63**(4), 105 (2017).
- M. Martin, D. Caliste, R. Cipro, R. Alcotte, J. Moeyaert, S. David, F. Bassani, T. Cerba, Y. Bogumilowicz, E. Sanchez, Z. Ye, X. Y. Bao, J. B. Pin, T. Baron, and P. Pochet, *Appl. Phys. Lett.* **109**(25), 253103 (2016).
- C. Shang, J. Selvidge, E. Hughes, J. C. Norman, A. A. Taylor, A. C. Gossard, K. Mukherjee, and J. E. Bowers, *Phys. Status Solidi A* **218**(3), 2000402 (2021).
- C. Hantschmann, Z. Liu, M. Tang, S. Chen, A. J. Seeds, H. Liu, I. White, and R. Penty, *J. Lightwave Technol.* **38**(17), 4801 (2020).
- J. C. Norman, D. Jung, Y. Wan, and J. E. Bowers, *APL Photon.* **3**(3), 030901 (2018).
- Z. Liu, C. Hantschmann, M. Tang, Y. Lu, J.-S. Park, M. Liao, S. Pan, A. Sanchez, R. Beanland, M. Martin, T. Baron, S. Chen, A. Seeds, R. Penty, I. White, and H. Liu, *J. Lightwave Technol.* **38**(2), 240 (2020).
- Y. Wan, D. Inoue, D. Jung, J. C. Norman, C. Shang, A. C. Gossard, and J. E. Bowers, *Photon. Res.* **6**(8), 776 (2018).
- A. Abdollahinia, S. Banyoudeh, A. Rippen, F. Schnabel, O. Eyal, I. Cestier, I. Kalifa, E. Mentovich, G. Eisenstein, and J. P. Reithmaier, *Opt. Express* **26**(5), 6056 (2018).
- M. Kasim, S. N. Elliott, A. B. Krysa, and P. M. Smowton, *IEEE J. Sel. Top. Quantum Electron.* **21**(6), 668 (2015).
- B. Dong, X. C. de Labriolle, S. Liu, M. Dumont, H. Huang, J. Duan, J. C. Norman, J. E. Bowers, and F. Grillot, *J. Phys. Photon.* **2**(4), 045006 (2020).
- Y. Xiong and X. Zhang, *IEEE J. Quantum Electron.* **54**(1), 1 (2018).
- S. Chen, W. Li, J. Wu, Q. Jiang, M. Tang, S. Shutts, S. N. Elliott, A. Sobiesierski, A. J. Seeds, I. Ross, P. M. Smowton, and H. Liu, *Nat. Photonics* **10**, 307 (2016).
- W. Luo, Y. Xue, J. Huang, L. Lin, B. Shi, and K. M. Lau, *Photon. Res.* **8**(12), 1888 (2020).
- M. S. Al-Ghamdi, P. M. Smowton, S. Shutts, P. Blood, R. Beanland, and A. B. Krysa, *IEEE J. Quantum Electron.* **49**(4), 389 (2013).
- M. Witzany, R. Roßbach, W.-M. Schulz, M. Jetter, P. Michler, T.-L. Liu, E. Hu, J. Wiersig, and F. Jahnke, *Phys. Rev. B* **83**(20), 205305 (2011).
- K. Paschke, G. Blume, N. Werner, A. Müller, B. Sumpf, J. Pohl, D. Feise, P. Ressel, A. Sahn, R. Bege, J. Hofmann, D. Jedrzejczyk, and G. Tränkle, *Opt. Rev.* **25**, 149 (2018).
- J. Xu, Y. Song, X. Yu, A. Lin, M. Kong, J. Han, and N. Deng, *Opt. Express* **24**(8), 8097 (2016).
- R. Fekrazad, A. Sarrafzadeh, K. A. M. Kalhori, I. Khan, P. R. Arany, and A. Giubellino, *Photochem. Photobiol.* **94**(4), 775 (2018).
- S. Shutts, S. Elliott, P. M. Smowton, and A. B. Krysa, *Semicond. Sci. Technol.* **30**(4), 044002 (2015).
- Z. Huang, M. Zimmer, S. Hepp, M. Jetter, and P. Michler, *IEEE J. Quantum Electron.* **55**(2), 1 (2019).
- Z. Li, C. P. Allford, S. Shutts, A. F. Forrest, R. Alharbi, A. B. Krysa, M. A. Cataluna, and P. M. Smowton, *IEEE Photon. Technol. Lett.* **32**(17), 1073 (2020).
- P. Dhingra, S. Fan, Y. Sun, R. D. Hool, B. Eng, and M. L. Lee, *Appl. Phys. Lett.* **117**(18), 181102 (2020).
- T. Zhou, M. Tang, G. Xiang, X. Fang, X. Liu, B. Xiang, S. Hark, M. Martin, M.-L. Touraton, T. Baron, Y. Lu, S. Chen, H. Liu, and Z. Zhang, *Optica* **6**(4), 430 (2019).
- J. Porsche, M. Ost, F. Scholz, A. Fantini, F. Phillipp, T. Riedl, and A. Hangleiter, *IEEE J. Sel. Top. Quantum Electron.* **6**(3), 482 (2000).
- W.-M. Schulz, R. Roßbach, M. Reischle, G. J. Beirne, M. Bommer, M. Jetter, and P. Michler, *Phys. Rev. B* **79**(3), 035329 (2009).
- T. Schwarzbäck, R. Bek, F. Hargart, C. A. Kessler, H. Kahle, E. Koroknay, M. Jetter, and P. Michler, *Appl. Phys. Lett.* **102**(9), 092101 (2013).
- Y. Chu, A. M. Mintairov, Y. He, J. L. Merz, N. A. Kalyuzhnyy, V. M. Lantratov, and S. A. Mintairov, *Phys. Lett. A* **373**(12–13), 1185 (2009).
- X. B. Zhang, R. D. Heller, M. S. Noh, R. D. Dupuis, G. Walter, and N. Holonyak, *Appl. Phys. Lett.* **83**(7), 1349 (2003).